CGU HS Committee on River Ice Processes and the Environment
21st Workshop on the Hydraulics of Ice Covered Rivers
Saskatoon, Saskatchewan, Canada, August 29-September 1, 2021

Field measurements of supercooling and anchor ice properties

Chuankang Pei[1], Jiaqi Yang[1], Yuntong She[1] and Mark Loewen[1]
[1]*University of Alberta,*
Department of Civil and Environmental Engineering,
University of Alberta, Edmonton, Alberta T6G 1H9
chuankan@ualberta.ca, jy9@ualberta.ca, yshe@ualberta.ca, mrloewen@ualberta.ca

River freeze-up is an important period with many dynamic and complex ice processes occurring in the supercooled, turbulent water. One such process is the evolution of anchor ice. Forming on the riverbed, anchor ice can accumulate to large thicknesses and release within a day but can also stay in place for multiple days. These dynamic anchor ice cycles have important implications for fish habitat, sediment transport, operations of hydropower stations and other water resources facilities. We conducted a field monitoring program during the 2020 freeze-up along the North Saskatchewan River in Edmonton, Alberta with the goal of improving our understanding of both supercooling and anchor ice properties. Temperature, depth and acceleration loggers were deployed in the study reach to capture supercooling events, water depth fluctuations and anchor ice formation and release. Sensors were mounted in shallow and deep water at several locations. A total of 34 anchor ice samples were collected during three site visits. The porosity of the samples was found to range between 32.3 % and 64.2 %, and the density from 329 to 624 kg/m^3. The supercooling properties in shallow and deep water are compared. Results show that the supercooling events that occurred in deep water had a longer duration and larger peak supercooling magnitudes on average. However, the number of events was roughly five times smaller in deep versus shallow water.

1. Introduction

In northern rivers, turbulent water becomes supercooled by heat exchange with colder air during the winter months. Supercooling and the presence of seed crystals lead to the formation of suspended frazil ice in the water column. Anchor ice can form either by deposition of adhesive suspended frazil ice particles to the river bottom or by in-situ nucleation on the bed material. As anchor ice grows in size, buoyancy forces may overcome the bonding force between anchor ice and the river bed which triggers the mechanical release of anchor ice. Warming of the water column may also weaken the bond, causing thermal release of anchor ice (Ghobrial and Loewen 2020).

The formation and growth of anchor ice require supercooling of the overlying water. The ice evolution, meteorological and hydrological conditions can all affect the river heat flux balance which makes supercooling a dynamic and complex process (Carstens 1966, Ye 2002). Several previous studies reported supercooling measurements that were gathered in the St. Lawrence River (Richard and Morse 2008, Richard et al. 2011). The differences between freeze-up and break-up supercooling events have been reported (Nafziger et al. 2013), and the shape of observed supercooling curves have been classified into three categories (Kalke et al. 2019). A study of the characteristics of the supercooling events in three Alberta rivers yielded an average peak supercooling of -0.016 ºC and a duration of 21 hours (Boyd et al. 2020).

Anchor ice formation is often initiated overnight during supercooling events and released when solar radiation warms the water above the freezing point (Kempema and Ettema 2011). The anchor ice process changes the river topography, impacts hydropower generation during winter seasons, and plays a significant role in sediment transport by anchor ice rafting (Jasek 2016, Kalke et a. 2015). Several studies have investigated the mechanism of anchor ice growth and release in detail (Kerr et al. 2002, Ghobrial and Loewen 2020). Numerical models have been developed to simulate anchor ice processes using semi-empirical equations which require anchor ice porosity as a calibration parameter (Shen 2010, Blackburn and She 2019). Field observations of anchor ice properties have been made by direct sampling from rivers or lakes (Parkinson 1984, Hirayama et al. 1997, Kempema and Ettema 2013, Jasek 2016, Stickler and Alfredsen 2009, Dubé et al. 2014) or by laboratory experiments (Andersson and Daly 1992, Qu and Doering 2007). The porosity of anchor ice was found to vary between 2% ~ 83.5% in field observations and 39% ~ 92% in laboratory experiments.

In this study, field measurements of hydro-meteorological conditions, surface ice concentrations, supercooling and anchor ice properties at various locations on the North Saskatchewan River during the 2020 freeze-up season are presented. A total of 34 samples were collected from released anchor ice pans during three site visits, the properties of anchor ice samples as well as the corresponding hydro-meteorological conditions are discussed in detail. Comparison of deep and shallow water supercooling properties are also presented to help improve our understanding of supercooling processes in natural rivers.

2. Study Sites and Methods

2.1 Study Sites and Instrumentation

The North Saskatchewan River (NSR) is a glacier-fed, regulated river that originates from the Canadian Rockies (Ghobrial and Loewen 2020). The winter discharge of NSR is strongly affected by the upstream Brazeau Dam and Bighorn Dam, these two dams are approximately 230 km and 430 km upstream of Edmonton, respectively (McFarlane et al. 2017). The average daily winter discharge at Edmonton is 126 m^3/s (Hicks 1997). Figure 1 shows the locations on the NSR where sensors were deployed and anchor ice samples were collected. Five locations inside the City of Edmonton were chosen as follows: Anthony Henday Bridge (Station 0 km), Terwillegar Park (Station 3.97 km), Quesnell Bridge (Station 10.53 km), Emily Murphy Park (Station 16.99 km), and Gold Bar (Station 27.87 km). Meteorological data was obtained from the Alberta Climate Information Service (ACIS) database (ACIS 2021). The closest ACIS weather station is the Edmonton South Campus UA station (Climate ID 3012220), see Figure 1. The hourly air temperature and solar radiation data from this station are used to analyze the influence of environmental conditions on supercooling and river ice processes.

Water temperature and water depth were measured using RBR Solo T (accuracy ± 0.002 ºC) temperature loggers and Van Essen Diver (accuracy ± 1 cmH2O) water level loggers sampling every 1 and 15 min, respectively. Both loggers were placed inside a protective mount as shown in Figure 2a. For the shallow water measurements, the mount was anchored to the riverbed by rebar pins in water depths that of ~60 cm. For deep water measurement, the mount was attached to a steel cable and lowered from the bridge located near the shallow mount location. The cable was then brought down to the shore and attached to a tree. In this study, four shallow water mounts were deployed at Anthony Henday Bridge, Quesnell Bridge, Emily Murphy Park and Gold Bar, respectively. Three deep water mounts were deployed at the Anthony Henday Bridge, Quesnell Bridge and Gold Bar, respectively. Unfortunately, the deep water mount at the Quesnell Bridge was lost and the one at the Anthony Henday Bridge was found moved close to the bank and completely buried by soft mud. The deep water mount at the Gold Bar location also moved from its original location at a depth of ~250 cm to shallower water but did not appear to be affected by mud.

Anchor ice samples were collected at Terwillegar Park and Emily Murphy Park during three site visits during the 2020 freeze-up period. Three shallow water mounts located at Quesnell Bridge, Emily Murphy Park and Gold Bar were equipped with Onset HOBO Pendant G acceleration and tilt data loggers sampling every 5 min to detect the presence of anchor ice. The idea is that prior to anchor ice formation the logger would move freely due to vortex shedding and fluctuating river flow velocities, generating fluctuating acceleration and tilt signals. However, when anchor ice forms on top of the sensor it is no longer free to move and the fluctuating signals disappear. As shown in Figure 2b, each mount had two Pendant G loggers installed on it, one oriented vertically and the other horizontally to detect the formation and release of anchor ice. The vertical and horizontal loggers were bolted to 5.8 and 4.3 cm springs, respectively that were fastened to the mount. The spring on the vertical logger at Gold Bar was found to be damaged when it was retrieved, therefore the data from this logger was discarded.

Figure 1. Measurement and anchor ice sampling locations on the North Saskatchewan River.

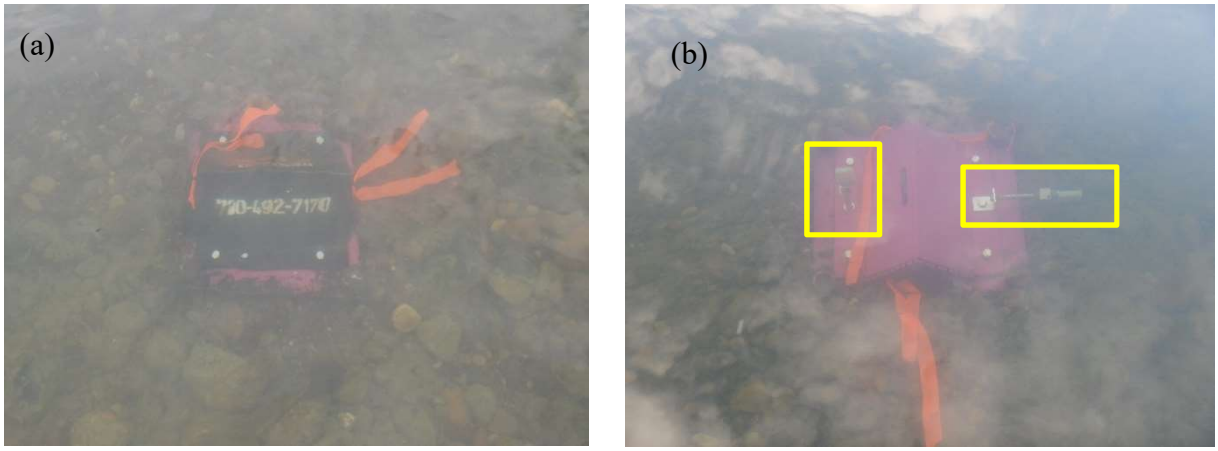

Figure 2. Images of shallow sensor mounts in the NSR. (a) A mount with only temperature and water depth loggers housed inside and (b) a mount housing temperature and depth loggers as well as two Pendant G loggers, outlined by the yellow rectangles.

2.2 Monitoring of Surface Ice Conditions

Surface ice conditions were monitored at all sites except Terwillegar Park using a trail camera (Reconyx HyperFire) with a 1 hour sampling interval. The trail cameras were mounted on trees near the deployment locations. Surface ice concentrations were computed using the University of Alberta (UA) Department of Earth and Atmospheric Sciences (EAS) Weather Station Camera images (EAS 2021). There are four high-resolution network cameras mounted on the top of the UA Tory Building at an approximate elevation of 122 m above the NSR water surface sampling images with a 15 min time interval. Images captured by the camera looking approximately 1.17 km downstream of the Emily Murphy Park location was used in this study. An example of a raw

image is shown in Figure 3a. The images were first filtered through a Convolutional Neural Network (CNN) based classifier to eliminate unusable blurred and night images. Then the images were rectified using an open-source MATLAB program called "g_rect" (Bourgault 2008). Finally, the rectified ice pan images and ice cover images were segmented using a U-Net convolutional deep neural network model (Ronneberger et al. 2017) and traditional Otsu thresholding techniques, respectively. Figure 3b-c are examples of geo-rectified and segmented binary images, respectively. The surface ice concentration was obtained by computing the percentage of white pixels in the segmented image.

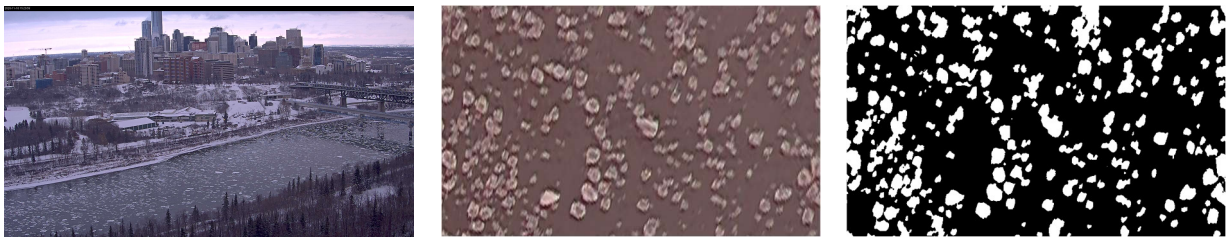

(a) Original image (b) Geo-rectified image (c) Processed image

Figure 3. Example of the image processing for EAS Camera. (a) original image, (b) geo-rectified image and (c) processed image.

2.3 Anchor Ice Sampling and Analysis Methods

In this study, the anchor ice properties of interest are porosity and density. The volume and mass of an anchor ice sample can be expressed as:

$$V_a = V_i + V_p + V_s \quad [1]$$

$$M_a = M_i + M_s \quad [2]$$

where V_a and M_a is the volume (m^3) and mass (kg) of an anchor ice, respectively; $V_i = V_w/0.917$ is the volume of the pure ice, V_w is the volume of the water melted from the ice, 0.917 is the density ratio of ice to water; M_i is the mass of the pure ice, V_p is the pore volume; V_s and M_s are the volume and mass of the sediments, respectively. The porosity and density of an anchor ice sample were calculated as follows:

$$e_a = \frac{V_a - V_i - V_s}{V_a - V_s} \quad [3]$$

$$\rho_a = \frac{M_a - M_s}{V_a - V_s} \quad [4]$$

where e_a is the porosity of an anchor ice sample, and ρ_a is the density of an anchor ice sample (kg/m^3).

Table 1 lists the details of the anchor ice sampling conducted on the NSR. During three site visits in November 2020, a total of 34 anchor ice samples were collected. Released anchor ice pans were visually identified by looking for ice pans that were clearly rafting sediments (i.e. had significant sediment concentrations). Samples were collected by scooping up a portion of the identified anchor

ice pan and then allowing the pore water to drain. The sample was then placed in a plastic bag as shown in Figure 4a. A simple workstation consisting of a modified cooler and two buckets was set up at the bank, see Figure 4b. The anchor ice volume (V_a) was obtained by submerging the bagged sample into the cooler and measuring the overflow in a graduated cylinder, see Figures 4b-c. Note that the volume of an anchor ice sample is the sum of the volume of ice, sediment and pores. After it is drained its mass is the sum of the ice and sediment. The sample was then transported in a sealed Ziploc bag to the laboratory for analysis. First, the mass of the anchor ice sample (M_a) was measured using a digital scale. The sample was then allowed to melt in the bags, the sediments were separated from the melted water, the mass and volume of the melted water were measured to calculate the pure ice mass (M_i) and volume (V_i). The separated sediments contained in the anchor ice sample were drained, the mass (M_s) and volume (V_s) of the sediments were then measured using a digital scale and a graduate cylinder, respectively.

Table 1. Summary of anchor ice sampling

Location	Sampling Date	Sampling Period	Samples Collected
Emily Murphy Park	12-Nov-2020	10:00 AM-12:00 PM	9
Terwillegar Park 1st	19-Nov-2020	10:00 AM-12:00 PM	8
Terwillegar Park 2nd	22-Nov-2020	10:00 AM-12:00 PM	17

Figure 4. Images showing the anchor ice volume measurement methodology, (a) anchor ice transferred into a plastic bag, (b) bagged sample submerged into cooler full of water using a pressing tool and, (c) measuring the volume of the overflow using a graduated cylinder

3. Results and Discussion

3.1 Anchor Ice Analysis

In Table 2 the porosity and density measurements of the anchor ice samples collected during the 2020 freeze-up are presented. The porosity for all samples ranged from 32.3 % to 64.2 % with a mean value of 52.3 %. The porosity of samples collected during the first two sampling trips (Emily Murphy and Terwillegar 1st) were comparable with mean values of ~ 49 % and maximums of ~ 60 %. The porosity for samples collected during the third sample trip (Terwillegar 2nd) is slightly larger with a mean and maximum of 56 % and 64 %, respectively. The density of all anchor ice samples ranged from 329 to 624 kg/m^3 with a mean value of 441 kg/m^3. The density of samples collected during the third trip (Terwillegar 2nd) is significantly smaller than the other two locations with a mean of 407 kg/m^3.

Figure 5 presents time series of air temperature and solar radiation, where the shaded area corresponds to the three anchor ice sampling trips. The average air temperatures during the three anchor ice sampling trips were -6.9, -12.8 and -4.5 ºC, respectively. It is noteworthy that the highest air temperature during the last sampling trip coincided with the largest average anchor ice porosity and lowest density.

Table 3 gives a summary of anchor ice porosity and density measurements from previous studies. The porosity of anchor ice was found to be between 2% ~ 83.5% for field observations on lakes and rivers, and 39% ~ 92% for laboratory experiments. The porosity of anchor ice in this study ranges from 32.3% to 64.2% with a mean value of 52.3%, which is comparable with the observations of Kempema and Ettema (2013) and Jasek (2016). The density range in this study is from 329 to 624 kg/m^3 which is similar to the Type I anchor ice samples reported by Stickler and Alfredsen (2009) that were associated with low turbulence and anchor ice growth predominantly on top of substrata with 'soft texture' and 'rough surface'. These conditions are qualitatively similar to the conditions that were observed during the sampling trips in this study.

Table 2. Porosity and Density of Anchor Ice Samples

Location	Samples	Porosity (%)			Density (kg/m^3)		
		Min.	Mean	Max.	Min.	Mean	Max.
Emily Murphy	9	32.3	49.1	60.4	374	475	624
Terwillegar 1st	8	35.9	48.7	59.4	374	475	596
Terwillegar 2nd	17	41.7	55.6	64.2	329	407	537
Combined	34	32.3	52.3	64.2	329	441	624

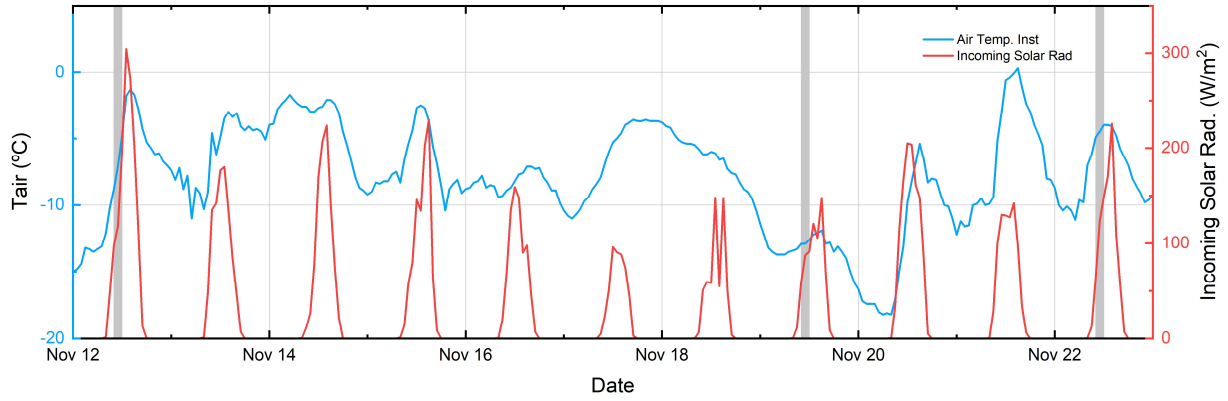

Figure 5. Time series of air temperature and solar radiation, shaded area corresponds to the anchor ice sampling time.

Table 3. Summary of previous anchor ice porosity and density measurements

Literature	Location	Porosity	Density (kg/m^3)
Parkinson (1984)	Lake Louise	70.7%-83.5% Average: 75%	N/A
Hirayama et al. (1997)	Niuppu River	24-47% (deduced)	240-700
Kempema and Ettema (2013)	Filed study of the wedge weir screen	42%-68% Average: 53%	N/A
Jasek (2016)	Peace River	30%-60% Average: 47%	N/A
Stickler and Alfredsen (2009)	2 natural rivers and 1regulated river	2%-61% (deduced)	Type I:360-600 kg/m^3 Type II: 633-900 kg/m^3
Dubé et al. (2014)	1 creek and 1 stream	Fixed-frazil ice: 24%-52%	N/A
Andersson and Daly (1992)	Lab experiment of water intake	39%-92% Average: 67%	N/A
Qu and Doering (2007)	Lab experiment	59%-88% Average: 73%	160-400 kg/m^3

Figure 6 presents time series of air temperature, solar radiation, water depth, water temperature and acceleration at Emily Murphy Park from 10-Nov-2020 to 14-Nov-2020. The shaded area in Figure 6 corresponds to the anchor ice sampling period. During this time period, the water was exposed to air temperatures well below zero for most of the time as shown in Figure 6a. The plot of surface ice concentration in Figure 6b shows that on 11-Nov the concentration rose to ~20% and subsequently varied between 17% to 21%. The depth was affected by hydropeaking cycles and fluctuated on a daily basis between 40 to 60 cm as shown in Figure 6c. Three complete supercooling events were identified from 10-Nov to 13-Nov, as shown in Figure 6d, with peak supercooling of -0.008 ºC, -0.027 ºC and -0.03 ºC, respectively. The first supercooling event on 10-Nov only lasted for 1.8 hours, but the latter two events both lasted for more than 24 hours. During the anchor ice sampling period, the water temperature was - 0.009 ºC at the start of the sampling and then increased briefly to 0.002 ºC at 11:22 before decreasing to - 0.004 ºC.

The time series of the acceleration in the flow direction measured by the horizontally and vertically installed Pendant G loggers are plotted in Figure 6e-f. Both signals were fixed at a constant value prior to the sampling period and then began fluctuating near the start of sampling at 10:00. The timing of the start of these fluctuations coincided with the field observations of anchor ice release. The steady water levels during the sampling period and for ~8 hours prior to the sampling period might be an indication that a thermal as opposed to a mechanical release event was occurring. The signal recorded by the vertical sensor fluctuated more than the horizontal sensor possibly due to its higher elevation above the bed and corresponding higher flow velocities. Both horizontally and vertically installed Pendant G loggers recorded multiple stationary time periods indicating potential anchor ice formation events. There is a relatively strong correlation evident between the

supercooling events and constant acceleration signals evident in Figure 7d, e-f. However, additional field measurements are needed to determine how reliably anchor ice formation and release can be detected using acceleration measurements of this type.

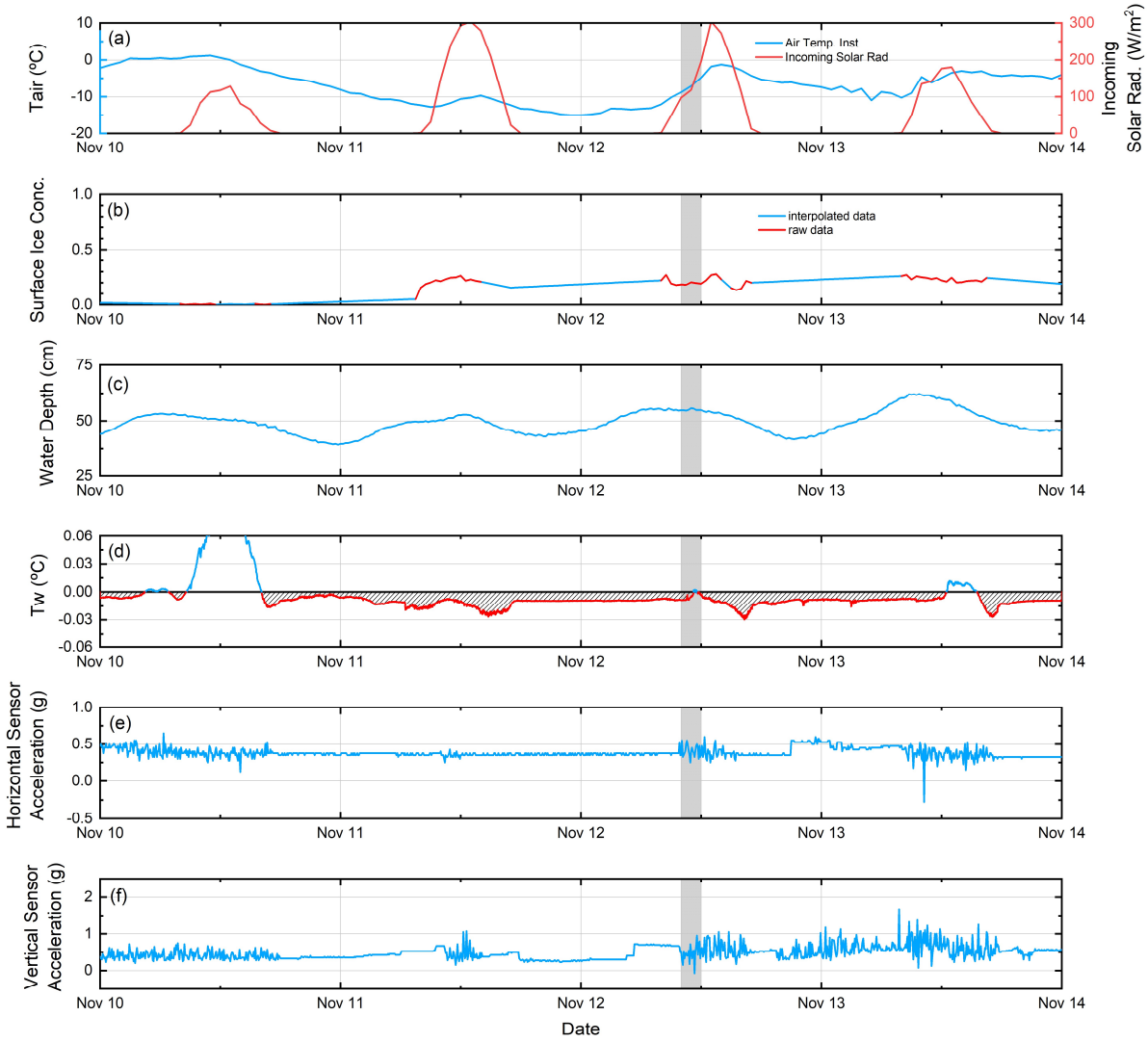

Figure 6. Time series of (a) air temperature and solar radiation, (b) surface ice concentration, (c) water depth, (d) water temperature, (e) horizontal Pendant G acceleration and (f) vertical Pendant G acceleration. Note that (c) ~ (f) are from sensors deployed at Emily Murphy Park, shaded area corresponds to the anchor ice sampling time.

3.2 Supercooling Observations

In Figure 7 time series of various measurements at the Gold Bar site from 8-Nov to 25-Dec, 2020 are presented, including the depth and temperature measurements collected by the deep and shallow sensors. As shown in Figure 7a the air temperature dropped to -18.2 ºC on 20-Nov. The trail camera images indicate that a complete ice cover was formed at this site on 21-Nov, as indicated by the shaded region, causing a ~120 cm increase in the depth that was recorded by both

sensors, see Figure 7c. The ice cover disappeared on 26-Nov and the depth recorded by both the shallow and deep sensors dropped accordingly. Between 26-Nov and 9-Dec, air temperatures fluctuated around zero and then dropped from a high of approximately 10 ºC on 9-Dec to a low of -20 ºC on 13-Dec. For the following two weeks air temperatures fluctuated dramatically and on 25-Dec a partial ice cover was formed with an open lead in the middle of the river.

In Figure 7b the difference between the depths measured by the deep and shallow sensor is plotted. Note that the shallower sensor was secured to the bed. The water temperature time series recorded by the deep and shallow sensors are plotted in Figures 7c-d, respectively. Supercooling events were first detected by both sensors on 9-Nov following low air temperature. Supercooling events in deep water were generally longer and less frequent compared to shallow water. The shallow sensor recorded frequent temperature fluctuations above and below zero, as can be seen in Figure 7d, likely due to the greater influence of varying solar radiation and air temperatures on the shallower water column. As a result, shorter and more frequent supercooling events were observed in the shallow water. A residual supercooling temperature was observed in deep and shallow water when the ice cover was in place.

The time series plot in Figure 7b of the depth difference between the deep and shallow mount shows that it varied considerably at times during the 2020 freeze-up period indicating that the deep mount was moving. This is understandable because the deep mount was not fixed to the river bed. Prior to 30-Nov the depth difference was ~200 cm with some minor variations indicating small movements of the deep sensor. However, on 30-Nov the depth difference decreased suddenly by ~120 cm indicating that the deep sensor had moved significantly closer to the left bank into shallower water. This movement may have been caused by natural processes (e.g. moving ice) or human interference (e.g. people pulling on the cable). Table 4 compares the peak supercooling and durations of events detected in deep and shallow water during these two time periods, before and after the deep sensor moved. During the first time period (8-Nov ~ 30-Nov) when the average water depth difference was ~200 cm, 11 events were recorded in deep water and 46 events were recorded in shallow water. The average peak supercooling at the deep and shallow locations was -0.023 and -0.011 ºC, respectively. The mean supercooling duration in deep water was 37.6 hours compared to 3.5 hours in shallow water. During the second time period (30-Nov ~ 25-Dec), the average water depth difference was 56 cm, 10 events were recorded in deep water and 51 events were recorded in shallow water. The average peak supercooling at the deep and shallow locations was -0.031 and -0.007 ºC, respectively. The mean supercooling event duration in deep and shallow water was 54.3 and 7.7 hours, respectively. This comparison shows that the number of supercooling events occurring in deep water was approximately five times smaller than in shallow water. The supercooling events that occurred in deep water were generally stronger with durations that were approximately an order of magnitude longer with peak supercooling temperatures that were two to four times larger in magnitude than the shallower water events. This result coincides with previous laboratory observations by Ye et al. (2004) that deeper flows produced longer durations of supercooling and larger peak supercooling.

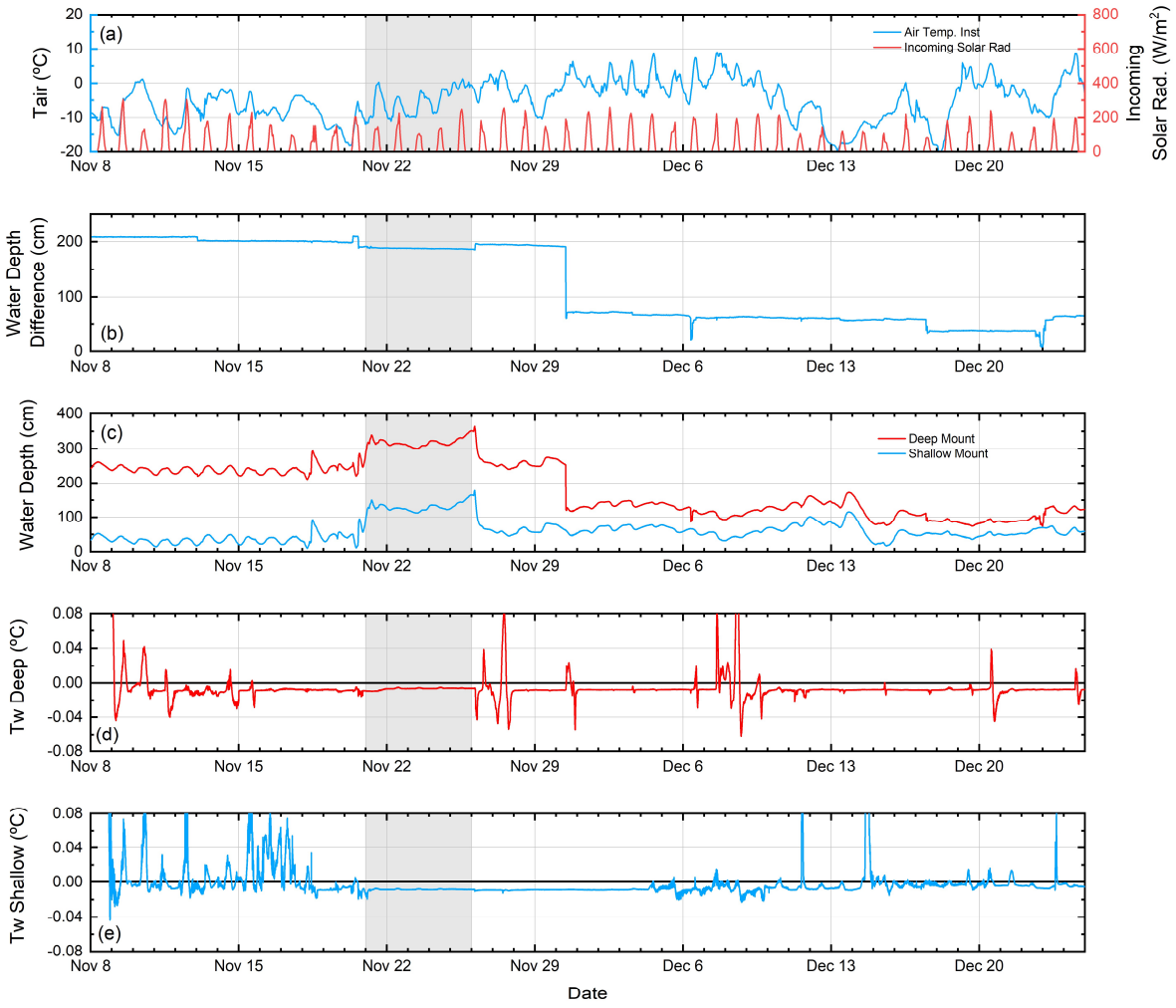

Figure 7. Time series of (a) air temperature and solar radiation, (b) water depth difference between deep and shallow mount, (c) water depth, (d) deep water temperature and (e) shallow water temperature. Note that plots (b) to (e) are data from sensors deployed at Gold Bar, the shaded area corresponds to the ice cover period.

Table 4. Summary of supercooling event properties observed at Gold Bar from 8-Nov-2020 to 25-Dec-2020.

Avg. Water Depth difference (cm)	Location	Events Count	Peak Supercooling (ºC)			Duration (hours)		
			Min.	Mean	Max.	Min.	Mean	Max.
200	Deep	11	-0.003	-0.023	-0.047	0.243	37.554	261.407
(8-Nov ~ 30-Nov)	Shallow	46	-0.002	-0.011	-0.044	0.173	3.474	48.432
56	Deep	10	-0.002	-0.031	-0.062	0.221	54.336	141.294
(30-Nov ~ 25-Dec)	Shallow	51	-0.002	-0.007	-0.023	0.175	7.693	46.457

4. Conclusion

Field measurements of supercooling and anchor ice properties were conducted at various locations on the North Saskatchewan River in Edmonton, Alberta during the 2020 freeze-up season. A total of 34 anchor ice samples were collected during three site visits. The porosity of anchor ice samples ranged from 32.3 % to 64.2 % with a mean value of 52.3 %. The density of anchor ice samples ranged from 329 kg/m^3 to 624 kg/m^3 with a mean value of 441 kg/m^3. A comparison of supercooling events detected by deep and shallow sensors at the Gold Bar site was presented. Results show that approximately five times fewer supercooling events occurred in deep water compared to shallow water. The supercooling events that occurred in deep water were significantly longer in duration and had larger peak supercooling magnitudes.

Acknowledgments

This research was supported by the Natural Sciences and Engineering Research Council of Canada (NSERC). We would like to thank Sean Boyd and Xun Hong for their help collecting anchor ice samples. We would also like to thank Perry Fedun for technical assistance. We would also like to thank Igor Jakab (Department of Earth & Atmospheric Sciences, University of Alberta) for providing the EAS camera images. The first author is partially funded by the China Scholarship Council (CSC) and the University of Alberta, respectively which is gratefully acknowledged.

References

Alberta Agriculture and Forestry, Alberta Climate Information Service (ACIS). 2021. Current and Historical Alberta Weather Station Data Viewer. Available from http://agriculture.alberta.ca/acis/weather-data-viewer.jsp [Accessed 10 May 2021].

Andersson, A., and Daly, S. F. 1992. Laboratory Investigation of Trash Rack Blockage by Frazil Ice. U.S. Army Corps of Engineers, Cold Regions Research and Engineering Laboratory CRREL Report 92-16.

Blackburn, J., & She, Y. 2019. A comprehensive public-domain river ice process model and its application to a complex natural river. Cold Regions Science and Technology, **163**, 44-58.

Bourgault, D. 2008. Shore-based photogrammetry of river ice. Canadian Journal of Civil Engineering, **35-1**, 80-86.

Boyd, S., Ghobrial, T. R., & Loewen, M. R. 2020. Observations of Supercooling in Rivers. 25th IAHR International Symposium on Ice, Trondheim, Norway, November 23-25, 2020, International Association for Hydro-Environment Engineering and Research.

Carstens, T. 1966. Experiments with supercooling and ice formation in flowing water. Det Norske Videnskaps-Akademi, **26-9**, 1-12.

Dubé, M., Turcotte, B., & Morse, B. 2014. Inner structure of anchor ice and ice dams in steep channels. Cold regions science and technology, **106**, 194-206.

Ghobrial, T. R., Loewen, M. R. 2020. Continuous in situ measurements of anchor ice formation, growth and release. The Cryosphere, **15**, 49-67.

Hicks, F., Cui, W., & Andres, D. 1997. Modelling thermal breakup on the Mackenzie River at the outlet of Great Slave Lake, NWT. Canadian Journal of Civil Engineering, **24-4**, 570-585.

Hirayama, K., Terada, K., Sato, M., Hirayama, K., Sasamoto, M., & Yamazaki, M. 1997. Field measurements of anchor and frazil ice. 9th Workshop on River Ice, Fredericton, NB,

Canada, September 24-26, 1997, CGU HS Committee on River Ice Processes and the Environment.

Jasek M. 2016. Investigations of anchor ice formation and release waves. 23rd IAHR International Symposium on Ice, Ann Arbor, Michigan USA, May 31 - June 3, International Association of Hydro-Environment Engineering and Research

Kalke, H., Loewen, M., McFarlane, V., & Jasek, M. 2015. Observations of anchor ice formation and rafting of sediments. 18th Workshop on the Hydraulics of Ice Covered Rivers, Quebec City, QC, Canada, August 18-20, 2015, CGU HS Committee on River Ice Processes and the Environment.

Kalke, H., McFarlane, V., Ghobrial, T. R., & Loewen, M. R. 2019. Field Measurements of Supercooling in the North Saskatchewan River. 20th Workshop on the Hydraulics of Ice Covered Rivers, Ottowa, ON, Canada, May 14-16, 2019, CGU HS Committee on River Ice Processes and the Environment.

Kempema E., Ettema R. 2013. Anchor ice and wedge-wire screens. 17th Workshop on River Ice, Edmonton, Alberta, Canada, July 21-24, 2013, CGU HS Committee on River Ice Processes and the Environment.

Kempema, E. W., Ettema, R. 2011. Anchor ice rafting: observations from the Laramie River. River research and applications, **27-9**, 1126-1135.

Kerr, D. J., Shen, H. T., & Daly, S. F. 2002. Evolution and hydraulic resistance of anchor ice on gravel bed. Cold Regions Science and Technology, **35-2**, 101-114.

McFarlane, V., Loewen, M., & Hicks, F. 2017. Measurements of the size distribution of frazil ice particles in three Alberta rivers. Cold Regions Science and Technology, **142**, 100-117.

Nafziger, J., Hicks, F., Thoms, P., McFarlane, V., Banack, J., & Cunjak, R. A. 2013. Measuring supercooling prevalence on small regulated and unregulated streams in New Brunswick and Newfoundland, Canada. 18th Workshop on River Ice, Edmonton, AB, Canada, July, 2013, CGU HS Committee on River Ice Processes and the Environment.

Parkinson F E. 1984. Anchor ice effects on water levels in Lake St. Louis, St-Lawrence River at Montreal. 3rd Workshop on River Ice, Fredericton, NB, Canada, June, 1984, CGU HS Committee on River Ice Processes and the Environment.

Qu, Y. X., Doering, J. 2007. Laboratory study of anchor ice evolution around rocks and on gravel beds. Canadian Journal of Civil Engineering, **34-1**, 46-55.

Richard, M., Morse, B. 2008. Multiple frazil ice blockages at a water intake in the St. Lawrence River. Cold Regions Science and Technology, **53-2**, 131-149.

Richard, M., Morse, B., Daly, S. F., & Emond, J. 2011. Quantifying suspended frazil ice using multi-frequency underwater acoustic devices. River research and applications, **27-9**, 1106-1117.

Ronneberger, O., Fischer, P., & Brox, T. 2015. U-Net: Convolutional networks for biomedical image segmentation. 18th International Conference on Medical Image Computing and Computer-Assisted Intervention, Munich, Germany, October 5-9, 2015.

Shen, H. T. 2010. Mathematical modeling of river ice processes. Cold Regions Science and Technology, **62-1**, 3-13.

Stickler, M., Alfredsen, K. T. 2009. Anchor ice formation in streams: a field study. Hydrological Processes, **23-16**, 2307-2315.

University of Alberta, Department of Earth and Atmospheric Sciences (EAS). 2021. EAS Weather Station. Available from https://www.ualberta.ca/earth-sciences/facilities/weather.html [Accessed 26 March 2021].

Ye, S. 2002. A physical and mathematical study of the supercooling process and frazil evolution. Doctoral dissertation, University of Manitoba.
Ye, S. Q., Doering, J., & Shen, H. T. 2004. A laboratory study of frazil evolution in a counter-rotating flume. Canadian Journal of Civil Engineering, 31-6, 899-914.